A zonal non-equilibrium approach to model temperature gradients during ventless bottom filling of pressurized cryotanks for natural gas-powered ships

Jonas Thiaucourt, Pierre Marty, Jean-François Hétet, Pascal Robert, Etienne Delaire

A zonal non-equilibrium approach to model temperature gradients during ventless bottom filling of pressurized cryotanks for natural gas-powered ships

Jonas Thiaucourt [a], PhD. Pierre Marty [a], Prof. Jean-François Hetet [a],
PhD. Pascal Robert [b], PhD. Etienne Delaire [b]

[a] Thermodynamics of internal combustion engines, Ecole Centrale de Nantes, LHEEA lab. (ECN/CNRS), Nantes, FRANCE

[b] French Maritime Academy (ENSM), Nantes, France

Corresponding author	Jonas Thiaucourt (PhD. Student)
E-mail address	jonas.thiaucourt@eleves.ec-nantes.fr
Full postal address	Ecole Centrale de Nantes 1 rue de la Noë, 44300 Nantes Jonas Thiaucourt, TSM (LHEEA)

No color should be used for any figures in print
Declaration of interests: none

Suggested referees:

Calogero Migliore	Gas and LNG Technology Manager at Repsol calogero.migliore@repsol.com Repsol, S.A., Centro de Tecnología Repsol, Paseo de Extremadura, Km 18, 28935 Móstoles, Madrid, Spain
David A. Wood	Principal consultant at DWA Energy Limited DWA Energy Limited Bassingham, Lincoln LN5 9JP, United Kingdom dw@dwasolutions.com
Maksym Kulitsa	FSRU Consultant, Odessa, Ukraine maksymkulitsa@gmail.com

Abstract

Liquefied Natural Gas (LNG) as a fuel is seen as a solution to curb harmful emissions in shipping and its quick uptake is now significant. New LNG bunkering scenarios are hence rising with a growing range of technical challenges. In this paper, a thermodynamic zonal model is established to assess the temperature gradients induced by a ventless bottom filling. The reservoir is divided into three control volumes. A condensation model at the liquid/vapor interface is proposed. Thermophysical properties are interpolated in tables allowing calculations with a good precision and a CPU time reduced of 68% compared to equation of state software direct calls. The non-equilibrium phenomenon of condensation blocking is highlighted. Then, the impact of the loading pressure is further investigated. As a result, it is shown that bottom filling rate at high pressure (around 11 bars absolute) can compete with vented filling techniques only if the tank can deal with strong spatial (liquid/vapor) and temporal temperature gradients, respectively of order 94.3 K and 0.19 K/s.

Key words: LNG fuel, no-vent filling (NVF), cryogenics, gas fueled ship

Content

Nomenclature

In some cases, it is unavoidable or simply practical to give symbols multiple definitions. From the context or subscripts it will be clear which definition applies.

A_{FS}	area of the free surface	m^2
C	Courant number	-
C_v (c_v)	heat capacity at constant volume (specific)	$J.K^{-1}mol^{-1}$ ($J.K^{-1}.kg^{-1}$)
D	thermal diffusivity	$m^2.s^{-1}$
D	diameter of the filling pipe	m
E (e)	energy (density)	J ($J.m^{-3}$)
e	insulation thickness	m
f	equation of state function	-
h	liquid height in the tank	m
h	specific enthalpy	$J.kg^{-1}$
H	height of the container	m
J	mass flow rate	$kg.s^{-1}$
k	hydraulic conductance	$kg.Pa^{-1}.s^{-1}$
L	length	m
m	mass	kg
P	pressure (all pressures are absolute)	kPa
q_h	condensation heat (latent + sensible)	$J.kg^{-1}$
R	cylinder radius	m
r	equatorial ellipsoid radius	m
S (s)	entropy (specific)	$J.K^{-1}$ ($J.K^{-1}.kg^{-1}$)
T	temperature	K
t	time	s
U (u)	internal energy (specific)	J ($J.kg^{-1}$)
V	volume	m^3
v	velocity	$m.s^{-1}$
W (w)	work (specific)	J ($J.kg^{-1}$)
x	position coordinate	m

Greek letters

Δx	space step	m
Δt	time step	s
λ	thermal conductivity	$W.m^{-1}.K^{-1}$
ρ	density	$kg.m^{-3}$
υ	specific volume	$m^3.kg^{-1}$
χ	vapor mass fraction	-
ϕ	flux density	$W.m^{-2}$

Subscripts

cd	condensation
comp	compression
eq	at equilibrium
ext	external
i	index variable for space at x=0, i=1
in	internal
is	isentropic
L	liquid
s	saturation
V	vapor

Superscripts

j	index variable for time at t=0, j=1

Acronyms

NVF	No-Vent Filling
LNG	Liquefied Natural Gas
NG	Natural Gas
EOS	Equation Of State
BOG	Boilf-Off Gas

Introduction

In the light of ever-tightening emission regulations, natural gas (NG) is perceived by ship-owners as a clean burning, available and affordable fuel choice [1]. NG is a complex mixture containing mainly methane (usually more than 80% in mass fraction) together with other hydrocarbon species, nitrogen, carbon dioxide and trace species [2]. For the sake of simplicity NG will be associated in this paper to pure methane. To save space onboard, NG is stored in insulated tanks at around -162°C under its liquid form known as LNG (Liquefied Natural Gas). In 2017, of the around 52 000 merchant ships, 103 LNG fueled ships (excluding LNG carriers) were in-service and 97 on order. This represents a year-on-year jump of +23% [3]. For NG operators, this trend is leading to new opportunities, innovative technical solutions and novel operations such as small scale bunkering [4]. On this subject, several arrangements are available: truck-to-ship, ship-to-ship or shore-to-ship transfers.

Shao and al. focused on the optimal time limit of ship-to-ship LNG bunkering by dynamic simulation, highlighting the link between the total Boil-Off Gas (BOG) and the bunkering time limit [5]. Grotle and al. discussed some operational challenges in LNG fuel systems and LNG handling on-board [6]. Unlike for large tanks, academic literature regarding small scale bunkering is scarce. As stated by Shao and al: "*Most of the earlier studies only focus on the large-scale LNG operations, and had overlooked the small-scale LNG fueled ships"* [5]. However, a state of the art review regarding LNG bunkering procedures for ships is proposed in [7]. Two small scale bunkering techniques exist.

The first one uses a vapor return line (see figure 1). This technique is straight forward as vapor is vented when the liquid level rises. A description of the bunkering procedure with a vapor return line can be found in [8][9].

A second technique can be used when LNG fueled ships are equipped with reservoirs designed to withstand pressure (type C [10]). They can be filled through a single hose with no vapor return line. This technique is known for hazardous cryogens as no-vent filling (NVF). A literature review about NVF can be found in [11][12].

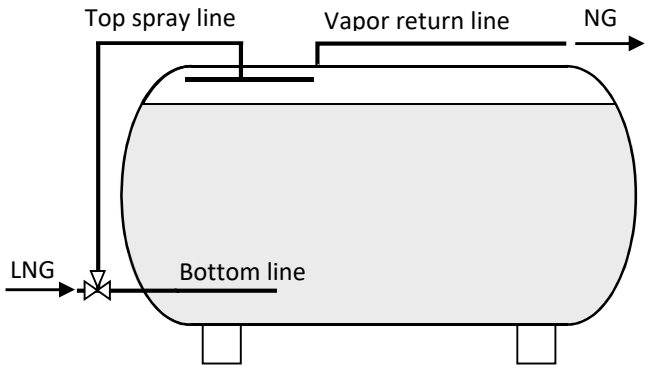

Figure 1 : Diagram of the LNG tank piping for bunkering

NVF of methane implies no potential leakage from vapor return pipes into air causing harmful emissions and fire risks. NVF also facilitates billing since the returned vapor energy content must not be deduced.

On the other hand, a high pressure in the receiving tank will make it harder for the LNG transfer to take place and the pump will have to work at a higher pressure and higher energy consumption. To avoid pressure build up, LNG top spraying is used to generate vapor collapse by condensation. However, loading rates are reduced during this operation impacting negatively the ship's downtime.

Achieving similar bunkering time for LNG and for conventional fuel is an important point for its development. To minimize downtime, a fast high-pressure bottom only NVF (no vapor return line nor top spraying) method could be used. This technique is already used in spatial industry, but it has been shown that during such filling an adverse thermodynamic effect between the vapor pressure and the condensation rate occurs: the condensation blocking effect [13]. This effect, resulting from a nonequilibrium state, generates important temperature gradients in the tank. Figure 2 summarizes the pros and cons of the existing methods compared to the vapor return line method.

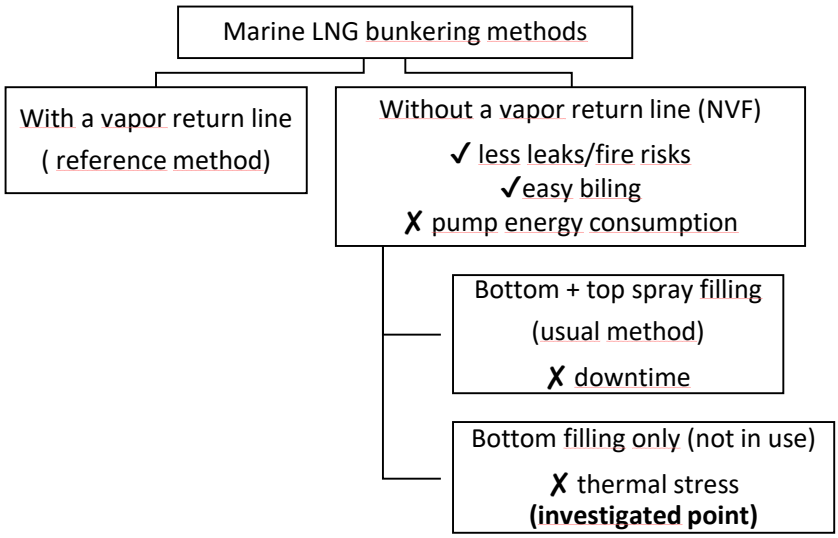

Figure 2 : Diagram of LNG bunkering methods with advantages/drawbacks

In 2017, the NASA released an open code for the simulation of cryogenic bunkering named LH2Sim [14]. LH2Sim models the condensation blocking effect. It shows good agreement with space shuttle refueling data [15] and the authors declare:

"We concentrate on a system of liquid hydrogen (LH2) filling motivated by the parameters of the space shuttle refueling system. Such a system can be considered as generic with respect to many existing and emerging liquid propellant loading schemes and cryogenic fluid management technologies."

In this paper, the NASA model is adapted to assess one drawback of the bottom only NVF: the temperature gradients in the tank. It is a key feature as thermal stresses must remain within limits set by manufacturers to maintain integrity.

In the first part, the tank geometry is described and modeled with three thermodynamic zones. Then, a self-consistent condensation model at the free surface is detailed. This model is similar to LH2Sim. To avoid unnecessary repetition, the paper only presents the work relevant to the adaptation of the model and kindly refers the reader to [11][12] for a more detailed description of the overall model. In the second part, the simulation details and results are analyzed. The impact of the external pressure (pump pressure) on the expected maximum liquid/vapor thermal gradient, the temperature rate of change and the bunkered volume is detailed. All the coding has been done using MATLAB and REFPROP [16].

1 Model development

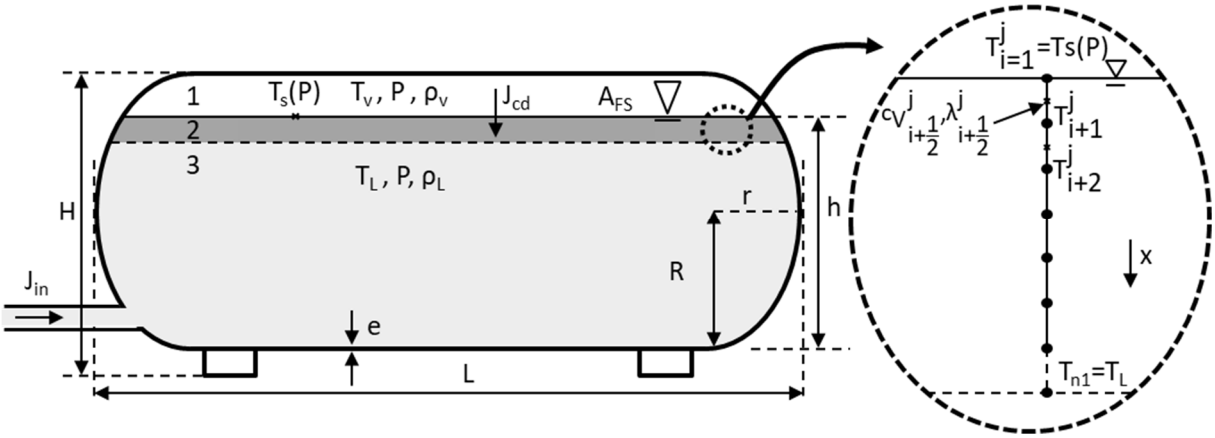

Figure 3 : Diagram of the tank geometry and the zonal model: zone 1 is the vapor ullage, zone 2 is a thin liquid layer below the interface and zone 3 is the bulk liquid zone.

1.1 The tank geometry

The tank geometry is based on a 40 ft. ISO container tank manufacturer datasheet [17].The reservoir is modelled as a cylinder with ellipsoidal heads. Its main characteristics are presented in table 1 and figure 3. The tank is meant to be operated roughly between 1 atm and a maximum working pressure (P) of 11 bars with a service pressure of 8 bars. The liquid volume (V_L) and the area of the free surface (A_{FS}) are functions of the liquid height (h) (equation 1-6). Figure 4 underlines the relation between the free surface area and the liquid volume against the liquid height. No corrections are made on the gauge relation [4]. This implies that:

- The vessel is assumed even keel (no trim, no list) and still;
- The thermal contraction or expansion of the tank is ignored;
- Inside the tank, the volume occupied by devices, for instance sensors, is neglected.

The tank nominal capacity is divided into three zones:

- Zone 1: the vapor ullage;
- Zone 2: the thin liquid layer at the vapor/liquid interface (also referred to as the Hashemi-Wesson layer [4]);
- Zone 3: the bulk liquid.

Symbol	Description	Value	Unit
Manufacturer specifications			
L+2r	Length of a 40 ft. container	12.192	m
2R	Width of a 40 ft. container	2.438	m
H	Height of a 40 ft. container	2.591	m
V	Nominal capacity	46	m^3
Constructed model data			
r/R	Ellipsoid aspect ratio	0.5	-
R	Equatorial radius	1.219	m
e	Insulation thickness	0.0981	m

Table 1 : Basic design LNG tank data

The liquid level-to-volume relation is expressed as:

$$V_L = V_{ellipsoid}(h) + V_{cylinder}(h) \quad (1)$$

$$V_{ellipsoid} = \frac{\pi r(3R - h)h^2}{3R} \quad (2)$$

$$V_{cylinder} = \left(L - 2(r + e)\right)\left[R^2 \cos^{-1}\left(\frac{R - h}{R}\right) - (R - h)\sqrt{2Rh - h^2}\right] \quad (3)$$

The liquid level-to-free surface area relation is expressed as:

$$A_{FS} = A_{FS_{ellipsoid}}(h) + A_{FS_{cylinder}}(h) \quad (4)$$

$$A_{FS_{ellipsoid}} = \frac{\pi r}{2}\sqrt{R^2 - |R - h|^2} \quad (5)$$

$$A_{FS_{cylinder}} = \left(L - 2(r + e)\right)\sqrt{R^2 - |R - h|^2} \quad (6)$$

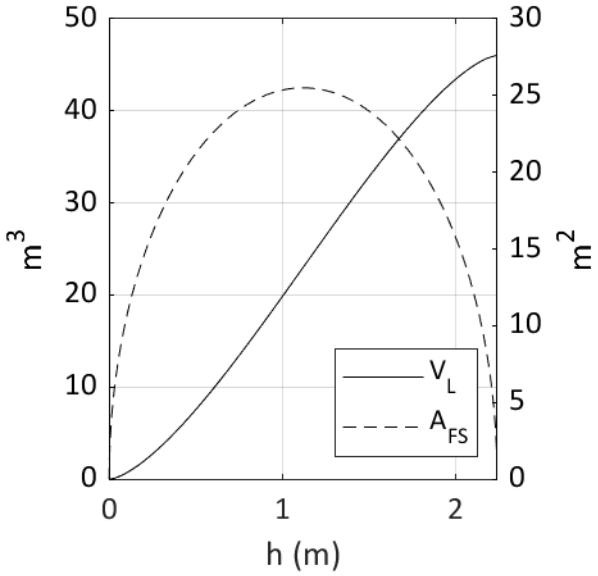

Figure 4 : Liquid volume and free surface area against the liquid height

1.2 Zone 2 condensation model and conservation equations

1.2.1 Zone 2 condensation model

In this part, the zone 2 condensation model is developed. Compared to LH2Sim, major differences are:

1. The free surface area is a function of the liquid level.
2. In the thin layer, the liquid conductivity (λ_L) and specific heat capacity (c_v) are functions of the temperature (T).
3. Real fluid equation of state is used to generate thermophysical properties.
4. The heat of condensation (q_h) is a pressure-dependent value.

1.2.1.1 Theoretical background

The zone 2 system energy conservation principle can be written as:

$$\frac{d}{dt}\iiint_{V(t)} e\cdot dV = 0 \qquad \textbf{7}$$

According to Leibnitz, the time variation rate of the energy integral over the volume is equal to the integral of the energy density time variation plus the density flux through its surface (8). Then, using Green-Ostrogradski theorem (9), it is possible to rewrite (7), as (10). Thanks to the continuum hypothesis, equation (10) remains valid on an infinitesimal volume leading to the local expression (11). In the scope of this study, the zone 2 is not subject to advection of particles since the upper boundary temperature (T_s) will always be higher than the lower one (T_L): $T_V>T_s>T_L$. The zone 2 liquid is still and so heat transfer occurs mainly by conduction. The energy flux through the surface is thermal power. Its contribution is defined by the flux density vector $\vec{\phi}$ ($e\vec{v}=\vec{\phi}$). For conduction, the latter is described by Fourier's law (12). Finally, mixing the law of behavior (12) and the conservation principle (11) leads to the well-known heat equation (13) as in [18].

$$\frac{d}{dt}\iiint_{V(t)} e\cdot dV = \iiint_{V(t)} \frac{\partial e}{\partial t}\cdot dV + \oiint_{A(t)} e(\vec{v}\cdot\vec{n})\cdot dS \qquad \textbf{8}$$

$$\oiint_{A(t)} e(\vec{v}\cdot\vec{n})\cdot dS = \iiint_{V(t)} \mathrm{div}(e\vec{v})\cdot dV \qquad \textbf{9}$$

$$\iiint_{V(t)} \left(\frac{\partial e}{\partial t} + \mathrm{div}(e\vec{v})\right)\cdot dV = 0 \qquad \textbf{10}$$

$$\frac{\partial e}{\partial t} + \mathrm{div}(e\vec{v}) = 0 \qquad \textbf{11}$$

$$\vec{\phi} = -\lambda_L \overrightarrow{\mathrm{grad}}(T) \qquad \textbf{12}$$

$$\frac{\partial e}{\partial t} - \mathrm{div}\left(\lambda_L \overrightarrow{\mathrm{grad}}(T)\right) = 0 \qquad \textbf{13}$$

The energy balance for the zone 2 (the studied system) can be written as:

$$\frac{\partial e}{\partial t} = \frac{\partial(\rho_L u)}{\partial t} \qquad \textbf{14}$$

According to Callen [19], considering the form u=u(T,υ) and using the chain rule to write how u changes with respect to [T,υ] leads to (15).

$$du = \left(\frac{\partial u}{\partial T}\right)_{\upsilon} dT + \left(\frac{\partial u}{\partial \upsilon}\right)_{T} d\upsilon \qquad \textbf{15}$$

The limited compressibility of liquid ($\upsilon_L \approx$ constant) leads to equation (16).

$$\begin{cases} du = c_{V_L}(T)dT \\ c_{V_L}(T) = \left(\frac{\partial u}{\partial T}\right)_{\upsilon} \end{cases} \qquad \textbf{16}$$

Rearranging (13) for case study leads to the partial differential equation (17).

$$\frac{dT}{dt}\rho_L c_{V_L}(T) - \mathrm{div}\left(\lambda_L(T)\overrightarrow{\mathrm{grad}}(T)\right)=0 \qquad \textbf{17}$$

1.2.1.2 Domain

The zone 2 is the top 30 cm liquid layer at the vapor/liquid interface. This thickness is sufficient to reduce the problem to a semi-infinite case (confirmed by results, see figure 9). Given the short time of the process and the thickness of the tank insulation, the heat leaks through the tank wall are neglected and therefor the problem is considered adiabatic (no edge effects are considered) [20]. Moreover, the layer is still thin enough to consider the top and bottom surfaces of the zone 2 equal. Finally, the problem is reduced to a 1D semi-infinite wall heat equation.

The temperature gradient is unknown but expected to be significant so λ_L, c_{V_L} are considered as functions of the temperature (20), (21). In this purpose, an interpolation method is proposed in annex. This method reduces CPU time by 68% compared to an Equation Of State (EOS) software direct calls. Keeping the simulation time around one-minute permits easy to run parametric studies.

Introducing the thermal diffusivity (D) (22) and the Courant number (C) (23), an explicit discretization scheme (18) is implemented as (19). An explicit method is chosen as it has proven to be an efficient way to deal with nonlinear differential equations. For stability issue, Δx is chosen such that $C < 0.25$ [18].

$$\rho_L c_{V_{L_x}}{}^t \frac{\left(T_x^{t+\Delta t}-T_x^t\right)}{\Delta t} - \frac{\left[\left(\frac{\lambda_{L}{}^t_{x+\frac{\Delta x}{2}}(T^t_{x+\Delta x}-T^t_x)}{\Delta x}\right)-\left(\frac{\lambda_{L}{}^t_{x-\frac{\Delta x}{2}}(T^t_x-T^t_{x-\Delta x})}{\Delta x}\right)\right]}{\Delta x} = 0 \qquad \textbf{18}$$

$$T_i^{j+1}=C^j_{i+\frac{1}{2}}T^j_{i+1}-(C^j_{i+\frac{1}{2}}+C^j_{i-\frac{1}{2}}-1)T^j_i+C^j_{i-\frac{1}{2}}T^j_{i-1} \qquad \begin{matrix}(x=(i-1)\Delta x)\\(t=(j-1)\Delta t)\end{matrix} \qquad \textbf{19}$$

$$\lambda_{L_i}{}^j=\lambda_L\left(\frac{1}{2}\left(T^j_{i+\frac{1}{2}}+T^j_{i-\frac{1}{2}}\right),P^j\right) \qquad \textbf{20}$$

$$c_{V_{L_i}}{}^j=c_{V_L}\left(T_i^j,P^j\right) \qquad \textbf{21}$$

$$D_{x\pm\frac{\Delta x}{2}}=\frac{\lambda_{L_{x\pm\frac{\Delta x}{2}}}}{\rho_L c_{V_{L_x}}} \qquad \textbf{22}$$

$$C_{x\pm\frac{\Delta x}{2}}=\frac{\Delta t D_{x\pm\frac{\Delta x}{2}}}{\Delta x^2} \qquad \textbf{23}$$

1.2.1.3 Initial and boundary condition

1.2.1.3.1 Initial condition

The pressure in the tank is assumed homogeneous but varies with time (transient). This assumption is made since differences in pressure potentials would induce momentum, energy, and mass transfer driving back to equilibrium in a very short time compared to the bunkering time. The hydrostatic pressure is a marginal term thus neglected. The initial

temperature profile (at t=0) is uniform in all the zones and equals the initial liquid saturation temperature (24).

$$T_i^1=T_s\left(P^1\right),\ \forall i \qquad \textbf{24}$$

1.2.1.3.2 Boundary condition

According to [13], the temperature at the interface is equal to the liquid saturation temperature at the tank pressure. It's a Dirichlet transient condition.

$$T_1^j=T_s(P),\ \forall j \qquad \textbf{25}$$

1.2.2 Condensation rate

Condensation occurs at the free surface, considered massless. Therefore, according [21], the heat released by condensation added to the one due to conduction is equal to the energy flux through that interface (26). Numerically, the right part of equation (26) is solved using the finite difference scheme. There is no calibration or accommodation coefficients required to assess the mass transfer as there is in the Lee model [22] or in the well-known Hertz Knudsen formula with the sticking coefficient. The condensation rate (J_{cd}) evolves proportionally to the free surface area. This is why horizontal tanks (large free surface area) perform better towards equilibrium in NVF than the vertical ones given the same operational conditions as reported in [12].

$$\begin{cases} \dfrac{J_{cd}q_h}{A_{FS}}=-\lambda_L\dfrac{\partial T}{\partial x},\ x=0 \\ q_h=h(T_V,P)-h(P,\chi=0) \end{cases} \qquad \textbf{26}$$

1.2.3 Conservation equations

The bunkering process is now considered. Figure 5 is a diagram of the bottom NVF dynamics: a virtual actuator connects two volumes (zone 1 and 3). The bottom one (zone 3) receives liquid, compressing in an isentropic way the upper vapor zone (zone 1). The latter, in response, exchanges heat at interface causing condensation. The tank is bottomed filled with LNG and its mass flow (J_{in}) equals the pressure difference ($P-P_{ext}$) times the pipe hydraulic conductance (k) (27). The zone 1 mass and energy balance are written respectively as (28) and (29). The vapor compression is assumed adiabatic reversible (isentropic). The liquid volume is updated as (30). Finally, the pressure is updated with the new vapor density (ρ_V) and specific internal energy (u_V) (31).

$$J_{in}=k(P-P_{ext}) \qquad \textbf{27}$$

$$\frac{dm_V}{dt}=-J_{cd} \qquad \textbf{28}$$

$$\frac{dU_V}{dt}=\frac{W_{comp_{is}}}{dt}-J_{cd}q_h \qquad \textbf{29}$$

$$\frac{dV_L}{dt}=\left(\frac{J_{cd}}{\rho_L}\right)+\left(\frac{J_{in}}{\rho_L}\right) \qquad \textbf{30}$$

$$P=f(\rho_V,u_V) \qquad \textbf{31}$$

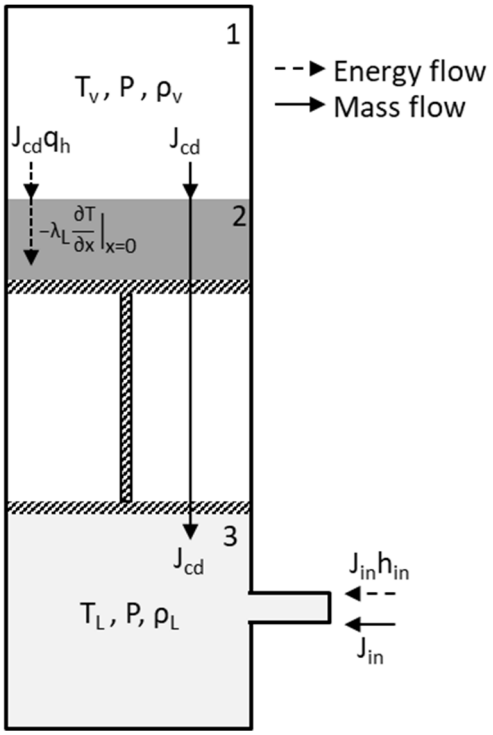

Figure 5 : Actuator analogy diagram representing heat and mass transfers during bottom NVF

2 Simulation and results

Initial pressure	P^1	101.325	kPa
External pressure	P_{ext}	506.625	kPa
Hydraulic conductance **	k	3.10^{-5}	$kg.Pa^{-1}.s^{-1}$
Diameter of the filling pipe	D	0.2	m
Heel volume	V^1	2.3	m^3
Time step	Δt^*	1	s
Total time	-	3600	s
Loading limit	V_L/V	90	%

Table 2: Simulation parameters

Using a realistic set of parameters (cf. Table 2), figure 6 shows the results of the simulation. The initial liquid volume (V^1) in the tank is 5% of the nominal capacity and the loading limit (V_L/V) is set at 90% of the nominal capacity. The inlet flow (J_{in}) is stopped if this threshold is reached. To highlight the condensation blocking effect, the liquid volume ratio (V_L/V) is plotted in parallel for a simple vented filling model (figure 6 a). In the vented model, the process is considered isobaric and isothermal. Vapor is withdrawn as LNG enters the tank to hold the pressure constant in the tank. It is considered as a reference ideal case.

Figure 6 b shows that the filling rate at the beginning of the simulation is high (around 100 m^3/h) due to the important pressure difference ($P_{ext} - P^1$). As the liquid flows upward in the tank, the vapor volume decreases and accordingly the pressure, saturation temperature and the condensation rate (J_{cd}) increase (figure 6 c and d). At this point, two competitive phenomena occur simultaneously: the heat and mass losses due to condensation are not high enough to compensate for the temperature increase due to compression. The condensation

* Time convergence checked

** Dimensionally consistent with speed, defined in [13]

is blocked by the conduction in the liquid phase: the LNG thermal conductivity is too low to maintain an equilibrium position.

The simulation results show that the condensation rate drops after a maximum of 0.069 m^3/h at 19'51'' (figure 6 b). As a consequence the vapor builds up resulting in a blocking of the filling. In this case, the level stalls at around 75%. From there, the condensation process will slowly generate a pressure drop enabling the filling to continue but at a very slow rate. In other words, the filling is led firstly by a fast gas compression step and then a slow heat conduction step.

When the filling stops (on figure 7 a and b at 438'39'' for $P_{ext} = 5$ bar the loading limit is reached), the whole system will slowly (order 1.10^2 hours) tend to a new equilibrium position. The final state can be predicted defining the tank as a global control volume and using a mass/energy balance ((32-35), and table 3). This final equilibrium state is in fact unlikely to be reached in the ship bunkering timescale.

$$\rho_{eq} = \frac{m^1 + \int J_{in} \cdot dt}{V} \quad \textbf{32}$$

$$U_{eq} = U^1 + \int \left(h_{in} J_{in} + \frac{1}{2} J_{in} v_{in}^2\right) dt \quad \textbf{33}$$

$$(P_{eq}, T_{eq}, \rho_{L_{eq}}, \chi_{eq}) = f(\rho_{eq}, u_{eq}) \quad \textbf{34}$$

$$V_{L_{eq}} = \left(1 - \chi_{eq}\right) V \rho_{eq} / \rho_{L_{eq}} \quad \textbf{35}$$

Practically, the bunkering flow rate is controlled (by the pumps) so that the LNG speed remains below 10 m/s to avoid friction losses and vaporization.

The loading limit with a vented fill is reached in 22'40'' (figure 6 a). Filling a 46 m^3 LNG tank in around 20' is a realistic scenario since the 40 m^3 tank on the MV Princess Isabella is bunkered in 15' [23]. For information truck-to-ship total bunkering time lasts around 2 hours (which include additional processes not modelled here but described in [24]) to bunker 50 m^3 with one truck.

ρ^1	ρ_{eq}	u_{eq}	P_{eq}	T_{eq}	$\frac{V_{L_{eq}}}{V}$
kg/m^3	kg/m^3	kJ/kg	kPa	K	-
22.8	380.7	2.05	106.4	112.3	0.90

Table 3 : Thermophysical data of the initial and final equilibrium states (Pext=5 bar) when the filling (Jin=0) is stopped at 90%.

To increase the bunkering rate, a simple operational measure is to increase the external feeding pressure (P_{ext}) (boosting pumps). A parametric study on this factor is now proposed. A set of simulations are launched with different values of P_{ext} (506.625 kPa, 709.275 kPa, 911.925 kPa and 1114.575 kPa).

Figure 8 a shows that for the reference pressure (P_{ext} = 506.625 kPa), over one hour, the maximum temperature difference encountered is 55.9 K and the maximum rate of temperature change is 0.04 K/s. This value can be compared to the tank safety specifications. For the last three studied P_{ext}, the maximum encountered temperature delta between the vapor ullage and the bulk liquid is respectively 71.4 K, 83.8 K and 94.3 K (figure 7 a); the

temperature maximum rate of change rises with the external pressure (respectively 0.08 K/s, 0.13 K/s and 0.19 K/s) (figure 7 a).

Figure 8 b shows that a higher initial external pressure will increase the loading limit after 1h (respectively to 0.78, 0.84, 0.87 and 0.89). In other words, a high external pressure implies that the liquid level blocks at a higher value.

Figure 8 c shows that a higher external pressure implies an increased entering flow resulting in a quicker liquid volume growth and an earlier appearance of the blocking point (the inflection of the liquid volume rise). Also, liquid volume in the tank after one hour evolves inversely with the external pressure.

Figure 8 d shows that globally, the deviation from the reference vented model regarding the filling rate is lower as the external pressure rises.

Also, this parametric study (figure 8 b and d) shows that, to fill the tank at a rate comparable to a vented reference model, an external pressure of 11 bars is required. However, doing so generates strong thermal spatial and temporal gradients (94.3 K and 0.19 K/s respectively).

From a practical point of view, the filling rate will be imposed by the maximum thermal stress allowable on the tank.

Figure 9 shows the temperature profile at the beginning and the end of the simulation. It confirms the assumption made: the thickness of zone 2 is enough to reduce the problem to a semi-infinite case.

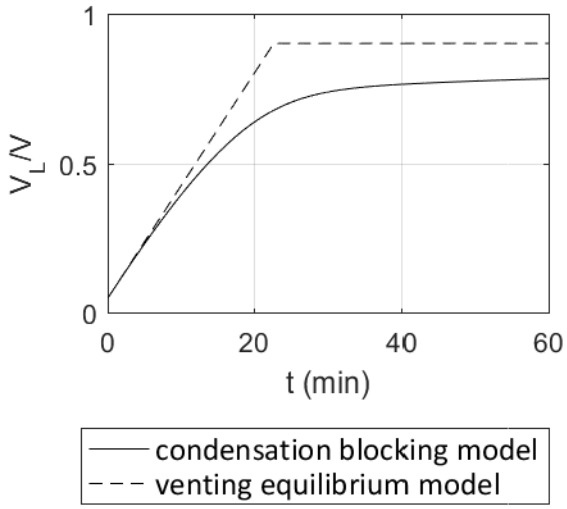

a) Liquid volume ratio (VL/V) history. The condensation blocking model stalls at 75%.

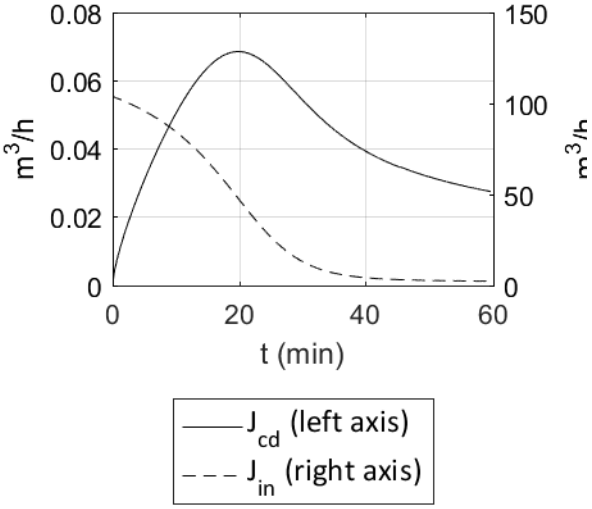

b) Condensation mass flow (J_{cd}) and inlet mass flow (J_{in}) history. A maximum condensation rate is reached at around 20'.

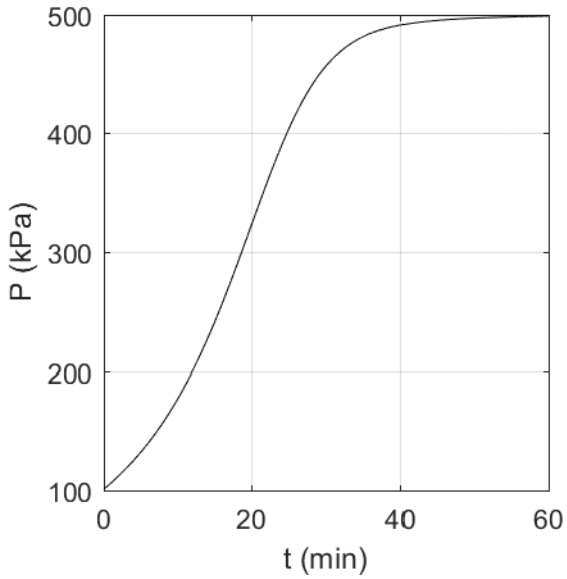

c) Pressure history in the tank driving the inlet flow.

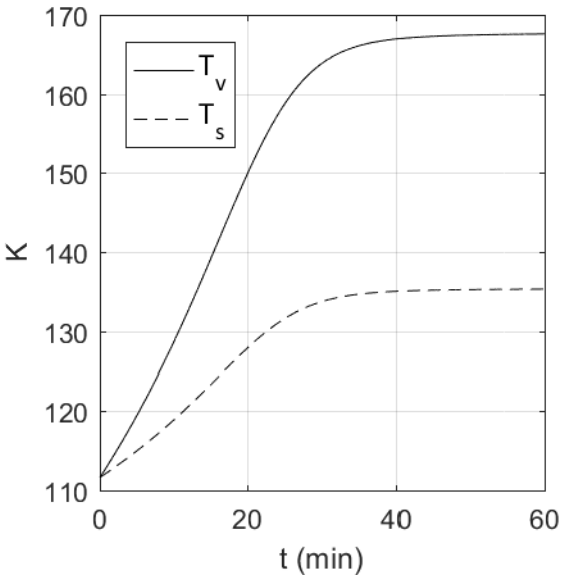

d) Temperature history in the vapor zone (T_v) and at the interface (T_s).

Figure 6 : Results

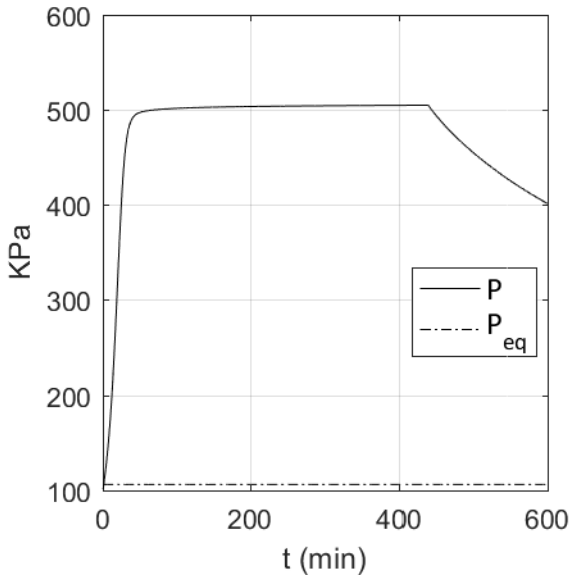

a) Pressure history: when the filling (J_{in}=0) is stopped at 90%, it tends to $P_{eq.}$

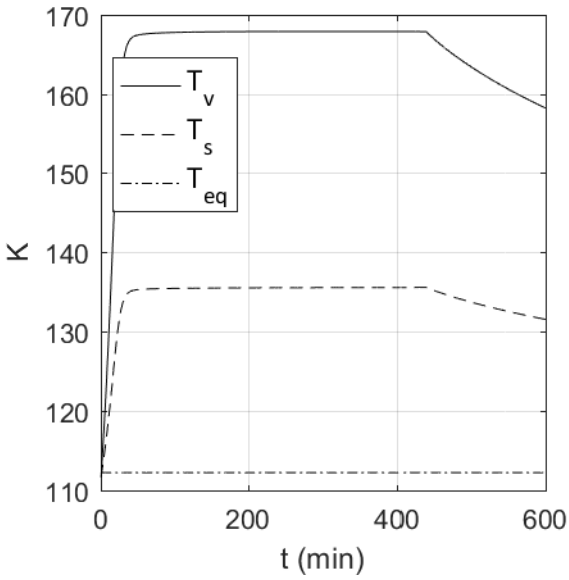

b) Temperatures history: when the filling (J_{in}=0) is stopped at 90%. T_V and T_s tend to T_{eq}.

Figure 7 : Times traces toward equilibrium (Pext=5 bar)

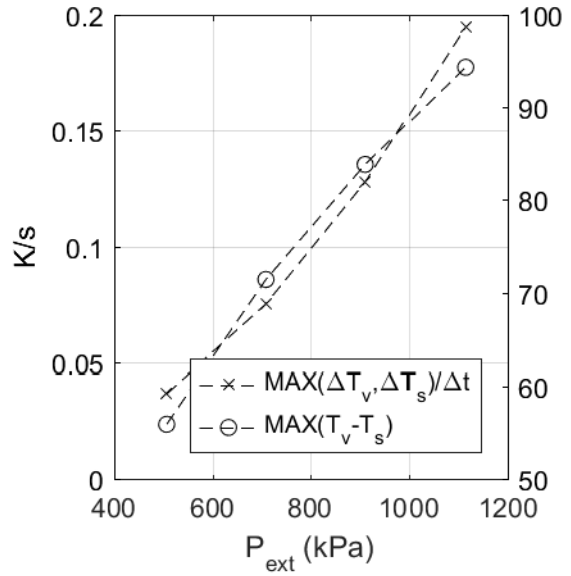

a) Maximum spatial and temporal thermal gradients against P_{ext} for 1 hour simulation

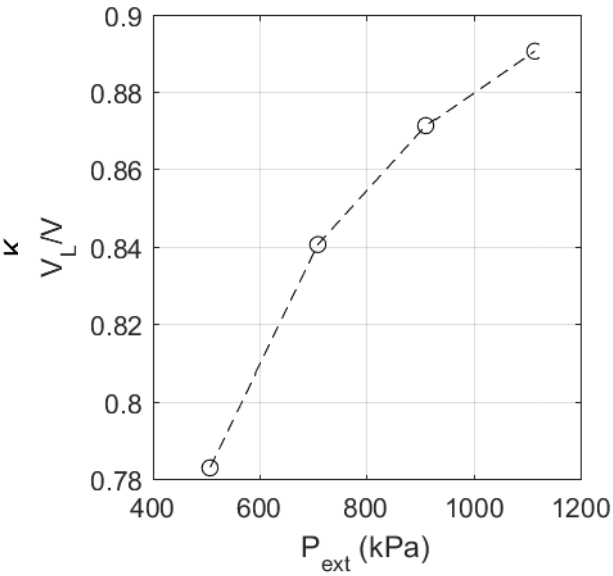

b) Liquid volume ratio after 1 hour against P_{ext}

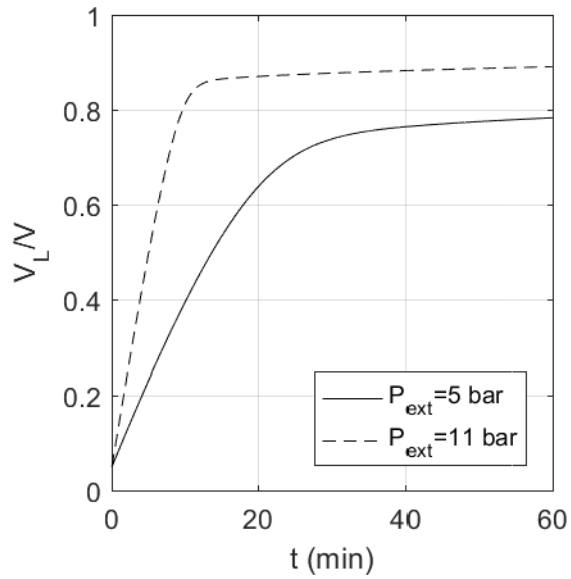

c) Liquid volume ratio history for two P_{ext}

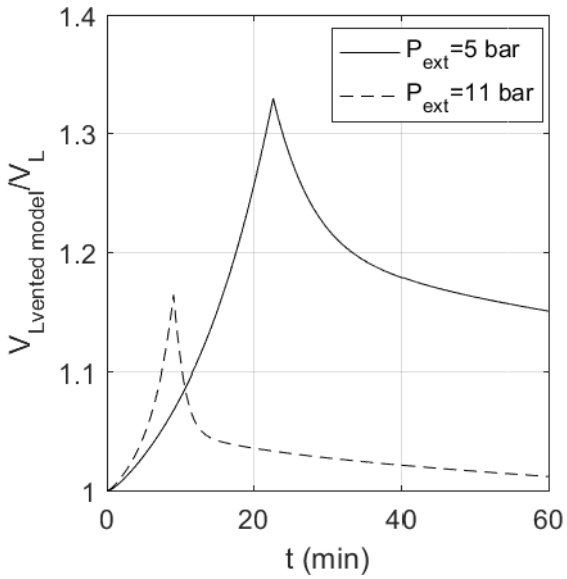

d) Reference vented model liquid volume over the liquid volume through time for two P_{ext}

Figure 8 : Results of the parametric study

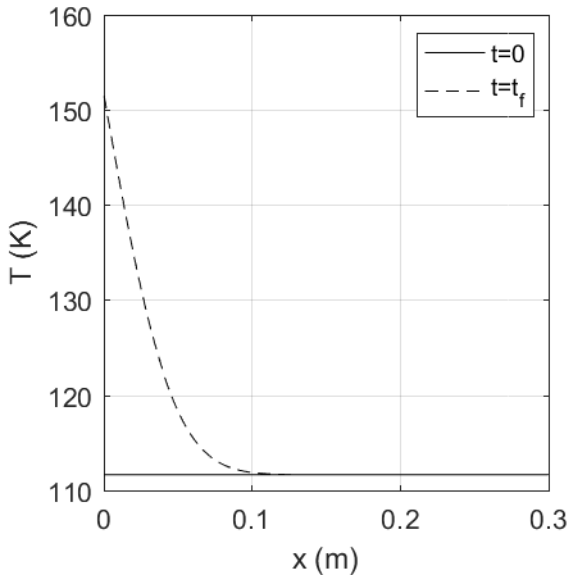

Figure 9 : Temperature profile in the zone 2 at the beginning and the end of the simulation (P_{ext}=11 bar)

Conclusion and future work

In this paper, a numerical model for a fast bottom only NVF of LNG tank onboard is proposed. It is based on a NASA cryogenic bunkering model. A fast interpolation method of the thermophysical properties for the heat conduction numerical scheme is implemented.

The results show that a high nonequilibrium effect limits the filling rate in the tank. Under an external pressure of 5 bars and for a realistic set of parameters, the loading level in the tank blocks at around 75%. From there, the remaining per cents toward completeness occur at a considerably slower rate. Full level can be reached at a vented filling rate with higher external pressure, but at the cost of strong thermal spatial and temporal gradients (up to 94.3 K and 0.19 K/s). A next step would therefore be to further investigate the capabilities of cryotanks to withstand the computed thermal stresses.
Also, it is reminded that this study is based on a NASA model validated for liquid hydrogen but supposedly applicable for other cyrogenic fuels such as LNG. However, comparison with experimental results should be carried out for confirmation. Doing so will clarify the feasibility of bottom fast NVF. Another option would be to try to mitigate the temperature gradients without reducing the flow rate. This could be done with an innovative concept: using column-loading pipe designed to exploit the Venturi effect, entraining vapor from the upper space and delivering it to the LNG at the bottom of the tank. This has been suggested recently in [25].

Annex: Thermophysical properties

An Equation Of State (EOS) can be defined as a set of relations, expressing intensive parameters in terms of the independent extensive parameters. Knowing all the EOS relations is equivalent to a complete knowledge of the system thermodynamic properties [19].

The GERG EOS [26], as implemented in REFPROP, is used to compute the thermophysical data needed. However, when called numerous times, it increases significantly the computational time of a simulation [27]. Therefore, thermophysical properties of interest are computed once, at various pressure/temperature to form a database on the studied domain. Then, in the numerical scheme, a linear interpolation on the scattered set of points is performed using a specific Delaunay triangulation (figure 10).

To make sure the number of data points is sufficient and well distributed, random points (P, T) are interpolated and then computed. From the error (36), an acceptance criterion on the cumulative distribution function (CDF) is set: CDF=1 for an error <0.1% (figure 11). The same method is used for c_V and λ.

$$error = \left| \frac{c_{V_{computed}} - c_{V_{interpolated}}}{c_{V_{computed}}} \right| \qquad 36$$

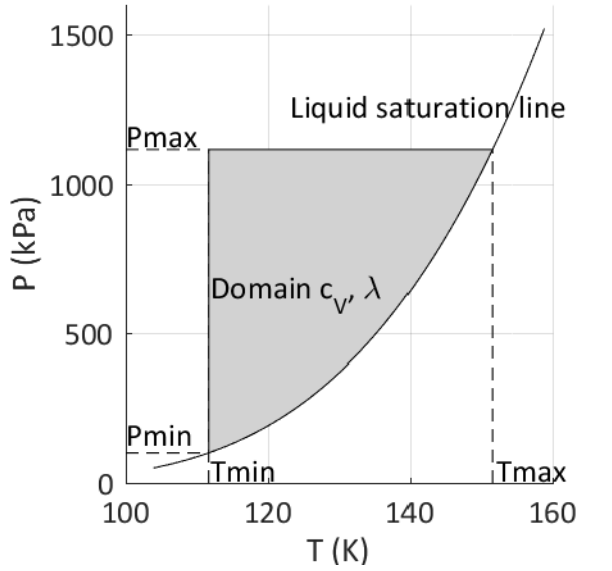

T_{min}	T_{max}	P_{min}	P_{max}
$T_s(P^1)$	$T_s(11\times P^1)$	P^1	$11\times P^1$

a) The domain of interest is the grey area (P^1=101.325 kPa).

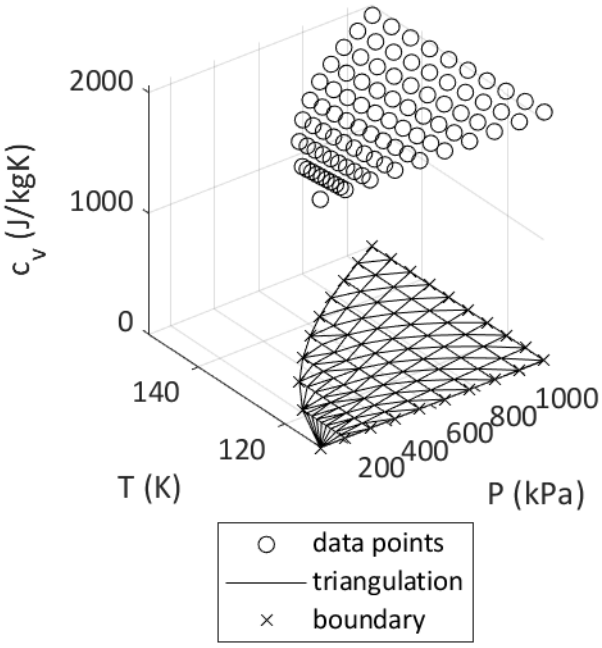

b) Inside the data domain, the values are interpolated using Delaunay triangulation method. This method is chosen since the hull is convex and relatively smooth.

Figure 10: Mapping domain for c_v and λ (a) and interpolation method (b)

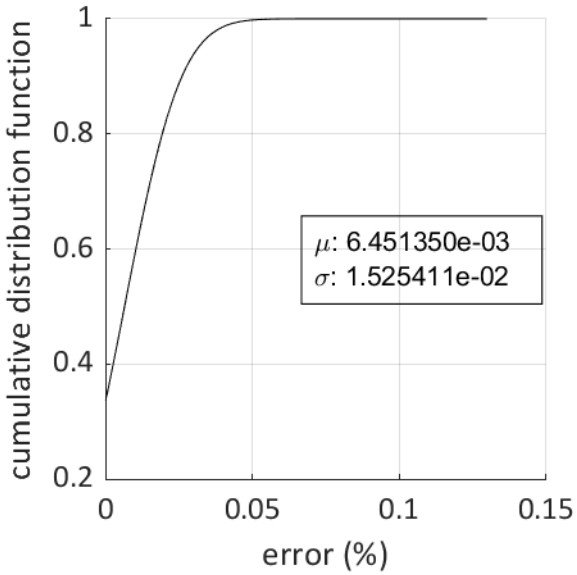

a) 640 random points are used to generate the CDF function of the error. The latter is used as an acceptance criterion for the database.

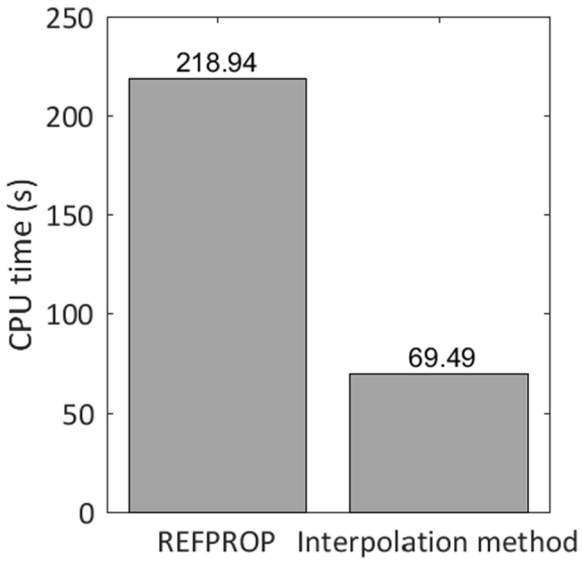

b) The CPU simulation time is reduced by 68.3% using the interpolation method rather than REFPROP calls in the heat conduction scheme. The time to generate the database is negligible (of order 0.1 s). Laptop: Intel-core i7-4700HQ @2.4Ghz (4 cores)

Figure 11: Acceptance criterion for the generated database (a) and CPU time saving results (b)

References

[1] DNV-GL, “In focus- LNG as ship fuel. Latest developments and projects in the LNG industry,” 2015.

[2] International Group of Liquefied Natural Gas Importers, “GIIGNL Annual Report,” 2017.

[3] M. Corkhill, “LNG-fuelled fleet hits 200 ship mark,” 2017. [Online]. Available: http://www.lngworldshipping.com/news/view,lngfuelled-fleet-hits-200-ship-mark_46977.htm. [Accessed: 16-Jul-2018].

[4] International Group of Liquefied Natural Gas Importers, “LNG Custody Transfer Handbook.” 2017.

[5] Y. Shao, Y. Lee, H. Kang, Y. Shao, Y. Lee, and H. Kang, “Dynamic Optimization of Boil-Off Gas Generation for Different Time Limits in Liquid Natural Gas Bunkering,” *Energies*, vol. 12, no. 6, p. 1130, Mar. 2019.

[6] E. L. Grotle, V. Aesoy, and E. Pedersen, “Modelling of LNG fuel systems for simulations of transient operations,” *Marit. Technol. Dev. - Proc. Int. Conf. Marit. Port Technol. Dev. MTEC 2014*, pp. 205–215, 2015.

[7] European Maritime Safety Agency (EMSA), “Guidance on LNG Bunkering to Port Authorities and Administrations,” 2018.

[8] ABS, “LNG Bunkering : Technical and Operational Advisory.” 2014.

[9] A. Slotte, J. Algell, and A. Ortberg, “Safety manual on LNG bunkering procedures for the Port of Helsinki,” 2017.

[10] International Maritime Organization, “IGF Code.” 2017.

[11] K. J. Kim, L. Jin, Y. Kim, and S. Jeong, “Experimental Investigation on No Vent Fill Process of Cryogenic Liquid,” in *The 27th International Ocean and Polar Engineering Conference*, 2017.

[12] C. Wang and R. Wang, “The effects of vertical and horizontal placement on no-vent fill of cryogenic insulated vessels,” *Cryogenics (Guildf).*, vol. 50, no. 8, pp. 480–485, 2010.

[13] V. V. Osipov and C. B. Muratov, “Dynamic condensation blocking in cryogenic refueling,” *Appl. Phys. Lett.*, 2009.

[14] J. Boschee and M. D. M. F. V. Smelyanskiy, “LH2Sim [Computer software].” 2017.

[15] V. V. Osipov, M. J. Daigle, C. B. Muratov, M. Foygel, V. Smelyanskiy, and M. D. Watson, “Dynamical Model of Rocket Propellant Loading with Liquid Hydrogen,” *J. Spacecr. Rockets*, vol. 48, no. 6, pp. 987–998, Nov. 2011.

[16] E. W. Lemmon, I. H. Bell, M. L. Huber, and M. O. McLinden, “NIST Standard Reference Database 23: Reference Fluid Thermodynamic and Transport Properties-REFPROP, Version 10.0, National Institute of Standards and Technology.” 2018.

[17] Trifleet, “TRIFLEET LNG SPEC 2017-10R2.” 2017.

[18] Y. Jaluria and K. E. Torrance, *Computational Heat Transfer*, Taylor & F. 2003.

[19] H. B. Callen, *Thermodynamics and an Introduction to Thermostatistics*, 4th print. 1985.

[20] J. Thiaucourt, K. Le Bail, and J. Hetet, “Impact of charged lng on its dynamic behaviour in a pressurized tank,” in *COFRET 2018*, 2018, pp. 1–6.

[21] V. Hovi, T. Pättikangas, and V. Riikonen, “Coupled one-dimensional and CFD models for the simulation of steam generators,” *Nucl. Eng. Des.*, vol. 310, pp. 93–111, Dec. 2016.

[22] W. H. Lee, “A Pressure Iteration Scheme for Two-Phase Modeling,” Los Alamos, 1979.

[23] J. Goodstein, “Maskinmesteren management and technology,” *August*, 2015.

[24] Bureau Veritas, “Guidelines on LNG Bunkering Guidance Note NI 618 DT R00 E,” 2014.

[25] K. Maksym and W. David A., “Floating storage and regasification units face specific LNG rollover challenges: Consideration of saturated vapor pressure provides insight

and mitigation options," *Nat. Gas Ind. B*, vol. 5, no. 4, pp. 391–414, Jul. 2018.
[26] T. Ajetunmobi, "LNG - Phase Behaviour," Imperial College London, 2010.
[27] J. M. Corberan, J. Gonzalvez, and D. Fuentes, "Calculation of refrigerant properties by linear interpolation of bidimensional meshes," in *IIR International Conference on Commercial Refrigeration/ Thermophysical Properties and Transfer Processes of Refrigerants,* 2005.